International Journal of Mechanical, Industrial and Aerospace Sciences
ISSN: 2517-9950
Vol:5, No:7, 2011

Detached-Eddy Simulation of Vortex Generator Jet Using Chimera Grids

Saqib Mahmood, Rolf Radespiel

***Abstract*—This paper aims at numerically analysing the effect of an active flow control (AFC) by a vortex generator jet (VGJ) submerged in a boundary layer via Chimera Grids and Detached-Eddy Simulation (DES). The performance of DES results are judged against Reynolds-Averaged Navier-Stokes (RANS) and compared with the experiments that showed an unsteady vortex motion downstream of VGJ. Experimental results showed that the mechanism of embedding logitudinal vortex structure in the main stream flow is quite effective in increasing the near wall momentum of separated aircraft wing. In order to simulate such a flow configuration together with the VGJ, an efficient numerical approach is required. This requirement is fulfilled by performing the DES simulation over the flat plate using the DLR TAU Code. The DES predictions identify the vortex region via smooth hybrid length scale and predict the unsteady vortex motion observed in the experiments. The DES results also showed that the sufficient grid refinement in the vortex region resolves the turbulent scales downstream of the VGJ, the spatial vortex core postion and non-dimensional momentum coefficient $\Delta R_{V_{xx}}$.**

***Index Terms*—VGJ, Chimera Grid, DES, RANS.**

I. Introduction

IN recent years it has been demonstrated that the use of active flow control (AFC) is promising to suppress flow separation on an aircraft. One possibility of active control of flow separation is the use of vortex generator jets(VGJ's). The VGJ are placed locally upstream of the seperation point to generate a longitudinal vortex for separation control through local changes in the near-wall stress field [1]. This longitudinal vortex engergizes the boundary layer by adding high momentum fluid from the outer region of the boundary layer towards the wall. In case of VGJ's the impact and effectiveness strongly depends on different flow control parameters such as the suitable set of pitch and skew angle of the VGJ relative to the main flow direction [2]. The usage of Reynolds-Averaged Navier-Stokes (RANS) method to simulate AFC configurations has grown rapidly in recent years. The numerical AFC predictions based on the RANS method through the use of eddy-viscosity based turbulence models is satisfactory in many cases and often provides good agreement with the experiments. Exceptions are caused by too high turbulent eddy viscosity in the vortex core regions [4] and hence vortex strength decays more rapidly than observed in experiments. An alternative approach towards the numerical AFC is to use Detached-Eddy Simulation (DES) models that belong to the Hybrid Reynolds-Averaged Navier-Stokes-Large Eddy Simulation (HRLES) family of turbulence modelling. The use of DES approach is considered promising at high-Reynolds number separated flows by a growing community [6]. One of the current mis-conception has been that DES should be applied with a somewhat coarser grid than LES in massive flow separations. This has sometimes led to inconclusive comparisons between LES and DES [7], [8]. Here we address the effects of numerical discretization errors by careful grid refinement. The present paper uses a current variant of the DES model i.e. the Improved Delayed DES (IDDES) turbulence model to simulate the effect of VGJ. This model has a non-zonal approach providing gradual continuous transition from RANS (attached-flows) to LES (detached-flows) via new definition of the subgrid length-scale that includes explicit wall-distance dependence, unlike earlier DES practice, which involves only the grid-spacings [9].

Saqib Mahmood is Research Assistant with the Institute of Fluid Mechanics,Technische Universität Braunschweig, 38106, Germany, e-mail: (sa.mahmood@tu-bs.de).

Rolf Radespiel is the Head of Institute of Fluid Mechanics, Technische Universität Braunschweig, 38106, Germany e-mail: (r.radespiel@tu-bs.de).

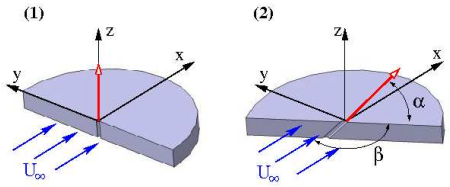

Fig. 1: Sketch of circular VGJ

II. Experimental Setup

The numerically investigated skewed VGJ as shown in Fig. 1 consists of a circular shape, hence the shape of the VGJ takes an elliptical opening on the flat plate surface.

The angle between the surface and the blowing direction is called the pitch angle α. The skew angle β is defined as the angle between the blowing axis and and the free-stream direction. For a circular hole both angles can be varied. The x-,y- and z-directions are defined as shown in Fig. 1. Additionally, U_∞ describes the stream-wise onset velocity of the flow in x-direction. In order to analyse the performance of a flow over a flat plate affected by a circular VGJ, detailed experimental campaign was carried out in the low-speed wind tunnel of the Institute of Fluid Mechanics, Technische Universität Braunschweig. This campaign established validation data to assess the flow prediction by numerical methods like RANS and DES. The experiments identified the range of efficient VGJ operation. That is the skew angle β is $90° - 105°$ and α is $30° - 45°$ [2], [3]. The present paper used the case of a VGJ with $\alpha = 45°$ and $\beta = 90°$ and a hole diameter of

$d/\delta = 0.073$, where δ is the measured boundary layer height at VGJ location. The resulting jet blows into positive y-direction. This VGJ was simulated exactly at flow conditions used during measurements. The experiments were performed in a closed-circuit atmospheric wind tunnel with a $6m \times 1.3m \times 1.3m$ test section. Free-stream velocities up to 55m/s can be reached. Inside the test section flat plate with an elliptical leading edge is installed at a height of $h/\delta = 3.42$ above the tunnel floor. The VGJ is located at approximate distance of $x/\delta = 53$ behind the leading edge of the flat plate and the resulting Reynolds number at this location is $Re_x = [7.67, 15.34] \cdot 10^6$ for a free-stream velocity $U_\infty = [25, 50]$m/s. Two velocity ratios $\lambda = u_j/U_\infty = [2.5, 5.0]$ were examined for both velocities [3], where u_j is the jet velocity. The numerical investigations focussed on a test case of $U_\infty = 25$m/s and $\lambda = 2.5$, using constant blowing. From the experiments, detailed flow field velocity measurement at four measuring planes downstream of the VGJ orthogonal to the free stream direction at locations $x/\delta = [0.571, 1.142, 2.283, 4.567]$, respectively, are available that were obtained using Stereoscopic Particle Image Velocimetry (3C2D-PIV) [3]. Furthermore in the lateral direction, i.e. in y-z plane, figures of merit, namely the non-dimensional momentum coefficient ΔR_{V_x}, in the four measuring planes provide a qualitative measure for the numerical simulations. ΔR_{V_x} is calculated as

$$\Delta R_{Vx} = \frac{\int_{y_1}^{y_2} \left[u^2 - u_0^2\right] dy}{\int_{y_1}^{y_2} u_0^2 dy} \quad (1)$$

The $index$ 0 denotes the undisturbed two-dimensional boundary layer flow and y_1 and y_2 denote the spanwise lower and upper integration limits for several measuring planes downstream of the jet actuator. This expression characterizes the global momentum tranpsort caused by the longitudinal vortex structure towards the wall [3].

III. Numerical Setup

A. Flow Solver

The numerical computations were carried out using the TAU-code [14], [15], which is a Finite-Volume based unstructured solver developed by the DLR. The code is based on the dual grid cell-vertex formulation and solves the compressible, three-dimensional RANS equations on both structured and hybrid grids composed of hexahedrons, prisms, tetrahedrons and pyramids. The inviscid terms in the governing equations were discretized in space using the second-order central scheme with matrix dissipation. In order to accelerate the steady state convergence, implicit backward-Euler time integration with a local time step and a LU-SGS implicit scheme with relaxation are coupled with multigrid and low-Mach number preconditioning. The TAU-code has the option of using Chimera grids with both structured and hybrid grids, which is useful for complex geometries [16], [17]. For the inflow into the VGJ the boundary condition `reservoir-pressure inflow` has been chosen with an inflow direction normal to the modelled inflow boundary. The total pressure at the inflow was defined to obtain the desired mass flux.

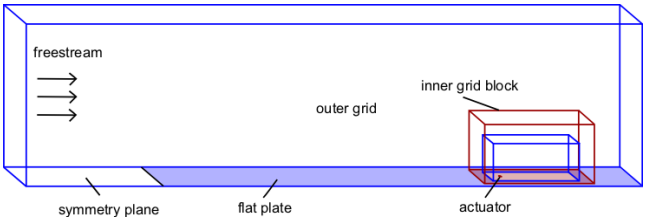

Fig. 2: Chimera grid setup for the flat plate

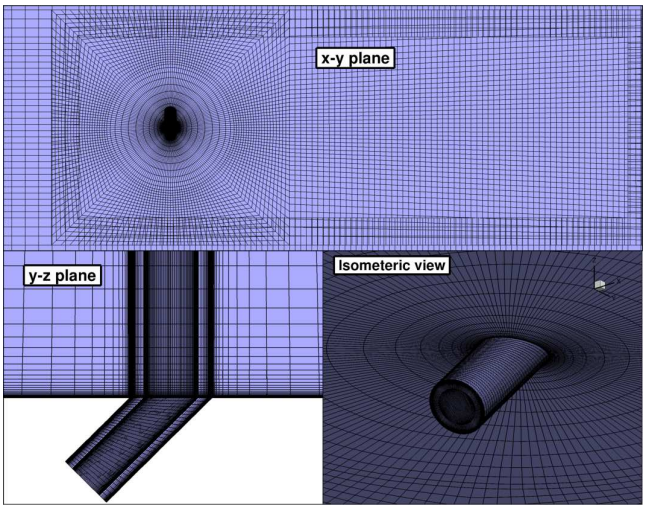

Fig. 3: Grid topology for the VGJ

B. Chimera Grid Setup

The Chimera grids were constructed with an approach of global and local grids. This approach was adopted to handle the large scaling differences between the size of the flat plate and the small scale VGJ. Additionaly this approach allowed to alter the structure of the local grids independently of the global grid. The local grid comprises the VGJ and the domain downstream of the VJG to capture the vortical flow phenomenon and the global grid is composed of the boundaries and limits of the domain including the setup of the manual hole cut that should fit the local grid at the particular position on the flat plate (see Fig. 2).

C. Grid Generation

The computational domain has an approximate size of 92δ x 2δ x 18δ in stream-wise, span-wise and wall-normal directions respectively, while δ is the boundary layer thickness at the actuator postion. The grid generation has been carried out using the commercial package Gridgen V15 [18]. Three different grids with fully structured hexahedral meshes consist of $4.0 \cdot 10^6$, $23.0 \cdot 10^6$ and $55.0 \cdot 10^6$ grid points respectively. The grid topology for the coarse grid is shown in Fig. 3. It shows three sub-figures with x-y & y-z planes in the vicinity of VGJ and an isometric view of the VGJ grid having O-type grid topology. The grid points distribution for the global and local grid is shown in Table I.

The computational resources from the high performance computing centre Norddeutscher Verbund für Hoch- und

TABLE I: Global and local grid distribution

description	grid1	grid2	grid3
local grid	$3.0 \cdot 10^6$	$18.0 \cdot 10^6$	$49.0 \cdot 10^6$
global grid	$1.0 \cdot 10^6$	$5.0 \cdot 10^6$	$6.0 \cdot 10^6$
total grid	$4.0 \cdot 10^6$	$23.0 \cdot 10^6$	$55.0 \cdot 10^6$

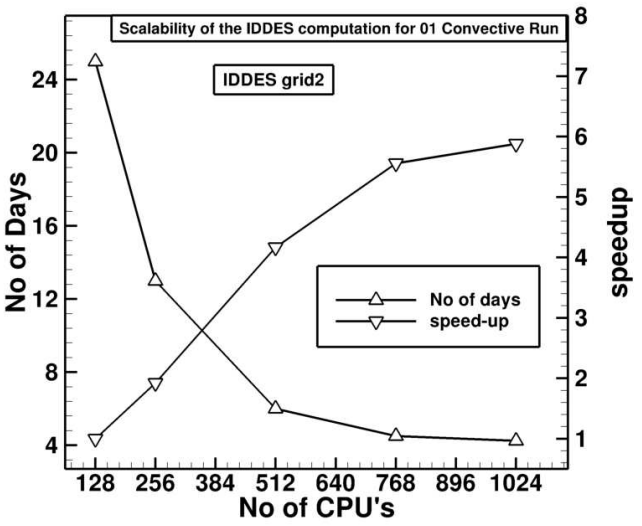

Fig. 4: Parallel scaling of DES computation

Höchstleistungsrechnen (HLRN) [19] were used with 128-Nodes (1024-CPU's) with 8-CPU's per node for grid2 and grid3. The TAU-code scales very well for the large parallel computations with the use of Chimera grid. The scalability of the DES computation over Chimera grids for one convective run (CR) is shown in Fig. 4, where 1 CR is the physical time required for the outer mean flow to convect through the domain of interest. For the present case, the domain of interest is an approximate distance having length of $x/\delta = 4.57$ behind the VGJ to characterize the evolution of the longitudinal vortex immersed in the boundary layer. The DES predicitions were obtained using the dimensionless timestep of 0.00156 ($1 \cdot 10^{-5}$ seconds) based on the jet velocity and the length of domain of interest behind the VGJ. The selected timestep yields a CFL number around one in the domain of interest corresponding to the strong vortical flow downstream of the VGJ.

D. Turbulence Modelling

RANS results shown here were obtained using two turbulence models: the Spalart-Allmaras one-equation model (S-A) [20] and the two-equation SST model of Menter (MSST) [21]. The S-A model is popular due to its ease of implementation, relatively low computational expenses, and good performance. The MSST model is a $k-\omega$ based model which accounts for the transport of the principal shear stress in adverse pressure gradient boundary layers.

1) DES Formulation: The DES simulation of VGJ over a flat plate has been carried out using the Improved Delayed DES (IDDES) [9] model which belongs to the Hybrid RANS-LES family. The present case used the IDDES model with S-A model as background RANS model in the attached flow regions and the detached flow is dealt with the LES formulation. The formulation involves the modification to the Delayed DES model [6] that resolve the log-layer mismatch and therefore, it is an essential implementation in theoretical terms. The two major elements are: a new definition of the subgrid length-scale that includes an explicit wall-distance dependence, unlike the usual LES practice which involves only the grid spacing, and an empirical RANS-LES hybrid function designed to provide a more successful coupling of the two approaches inside attached boundary layers.

The new definition of the subgrid length scale is given as:

$$\Delta = min\{max[C_w d_w, C_w h_{max}, h_{wn}], h_{max}\},$$

where h_{wn} is the grid step in the wall-normal direction and C_w is an empirical constant set equal to 0.15 based on a well-resolved LES of the developed channel flow. RANS-LES hybridization of the model couples the two approaches via introduction of a hybrid turbulent length scale based on the following blending of the RANS and LES length-scales:

$$\tilde{l} = f_{hyb}(1 + f_{restore}\Psi) l_{RANS} + (1 - f_{hyb}) C_{DES} \Psi \Delta,$$

where Δ is the subgrid length-scale defined by the above expression and C_{DES} is the empirical constant of the LES branch of DES [10], [11], while f_{hyb} and $f_{restore}$ are the blending functions used in the definition of the hybrid length scale. In accordance with the general DES concept [11], [12], [13] in order to create a hybrid model, the hybrid length-scale $\tilde{l}$ will be substituted into the background RANS model in place of the RANS length scale, l_{RANS} , explicitly or implicitly involved in any such model. For instance concerning the current paper, for the S-A model, the length scale is equal to the distance to the wall $l_{RANS} = d_w$ while for the MSST model, the length scale is $l_{RANS} = k^{1/2}/(C\omega)$.

2) DES Functionality without flow control: The functionality of the S-A IDDES model is first tested on a flat plate without flow control device. Fig. 5 shows the behavior of the S-A IDDES model at stream-wise position of $x/\delta = 0.571$, where z/δ is the wall-normal position. Fig. 5 shows that the S-A IDDES model preserves the eddy viscosity by shielding the boundary layer edge and the model reproduces the same results obtained with the S-A RANS approach. Simliarly Fig. 6 shows the mean logarithmic velocity profiles computed by the S-A RANS and S-A IDDES model at $x/\delta = 0.571$ downstream of the VGJ. The IDDES model reproduces the RANS results both in the "'inner"' and "'outer"' log-layer by protecting the boundary layer in the RANS (attached) region.

IV. Results

A. Grid Effects and Flow Field

RANS predictions shown here were obtained through grid convergence study detailed in [4] and grid1 was used as the grid independent solution. So grid1 is selected as the "base" grid for the DES computations as the grid fulfills the requirement of the IDDES model to have structured and isotropic cells in the LES region (see Fig. 3).

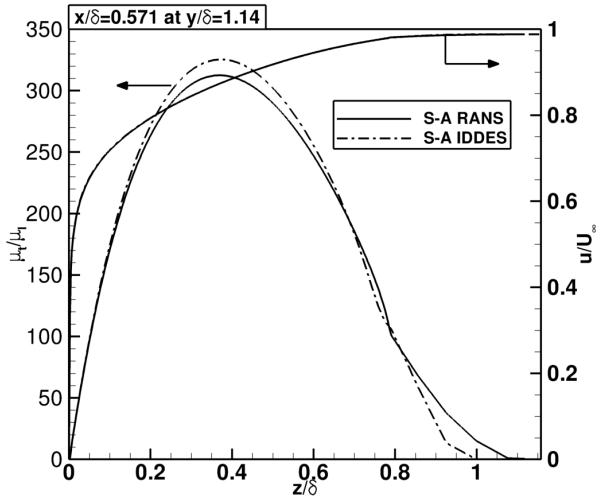

Fig. 5: Boundary layer shielding at x/$\delta = 0.571$,downstream of the VGJ

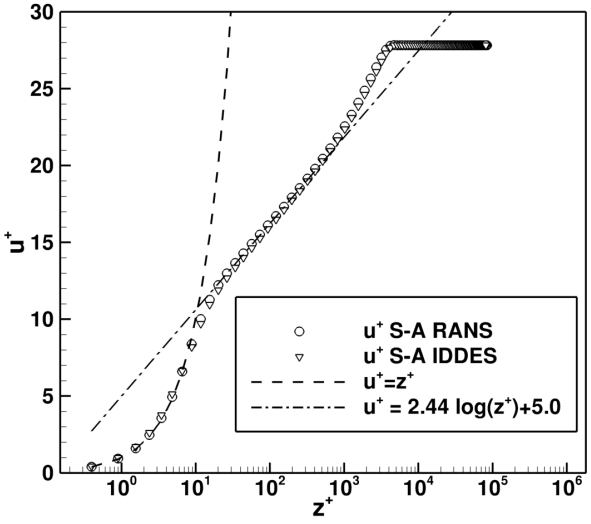

Fig. 6: Logarithmic velocity profile at x/$\delta = 0.571$

The computation on grid1 with S-A IDDES shows the general applicability of the method, as the depicted length-scale ratio l_{IDDES}/l_{RANS} correctly distinguishes the RANS and LES regions downstream of the VGJ at $x/\delta = 0.571$ as shown in Fig. 7. In the figure, y/δ and z/δ represent the normalized span-wise and wall-normal directions respectively. The results show that the IDDES model detects the vortex region quite well and locally extracted eddy-viscosity and l_{IDDES}/l_{RANS} profiles at $y/\delta = 0.114$ confirmed the boundary layer shielding in the RANS region and dropping of eddy-viscosity along with the length-scale in the LES region. Fig. 8 shows the iso-surfaces of the Q-criterion (second-invariance of velocity gradient tensor) colored by the normalized stream-wise velocity computed over grid1. The dense grid is the local grid and the coarse grid is the global grid out of the focus region of vortex. However, the visualisation of vortices by an iso-surface of the Q-criterion in Fig. 8 mainly reveal large

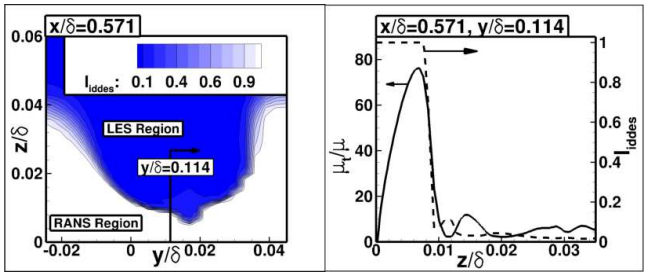

Fig. 7: Vortex detection via hybrid length scale

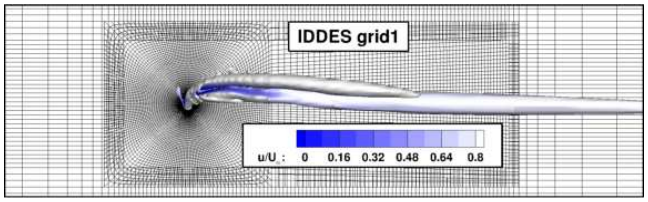

Fig. 8: Iso-Surface of the Q-criterion coloured by the normalized stream-wise velocity computed on grid1.

structures due to the vortical mean flow, whereas only few, rapdily decaying small-scale turbulent structures are observed. It was therefore concluded that a grid refinement is required to resolve an appropriate amount of turbulent stresses in the LES region. A systematic refinement by a factor of 2 in each direction in the crucial, inner Chimera part of the mesh led to grid2 with about $23.0 \cdot 10^6$ points. In a third step a local grid refinement between $x/\delta = (-0.571) - (+0.571)$ was performed that resulted in grid3 with $55.0 \cdot 10^6$ points respectively. The respective flow visualisation in Fig. 9 shows that these grid refinements lead to resolved turbulent structures in the domain of interest. It can be seen from the result that the grid resolution with grid2 was still not enough to generate strong turbulent motion as the iso-surfaces show only large structures. On the otherhand, grid3 with the local refinement downstream of VGJ produced a range of large vortices and small vortical structures and this caused strong turbulent mixing downstream of the VGJ. Another important feature observed in this figure is that the resolved vortex with grid3 appeared closer to the wall in comparison with the grid2.

Fig. 10 shows the comparison between the experiment and numerical data through normalized stream-wise, span-wise and wall-normal mean velocity contours downstream of the VGJ at $x/\delta = 0.571$ respectively. The last column in Fig. 10 represent the instantaneous data of three velocity components for IDDES grid3. While S-A RANS and MSST RANS show steady-state results, IDDES grid2 and IDDES grid3 refers to results obtained after an initial settling phase and time averaging over 10 CR's. The results show that the DES performance in the cross-flow plane improves as a result of grid refinement. It can be concluded that the IDDES grid3 and MSST RANS yield the best result in comparison with the experiment. S-A RANS and IDDES grid2, on the other hand, predicted a slightly higher vortex core as seen in the stream-wise velocity contour plots. Similarly, S-A RANS and

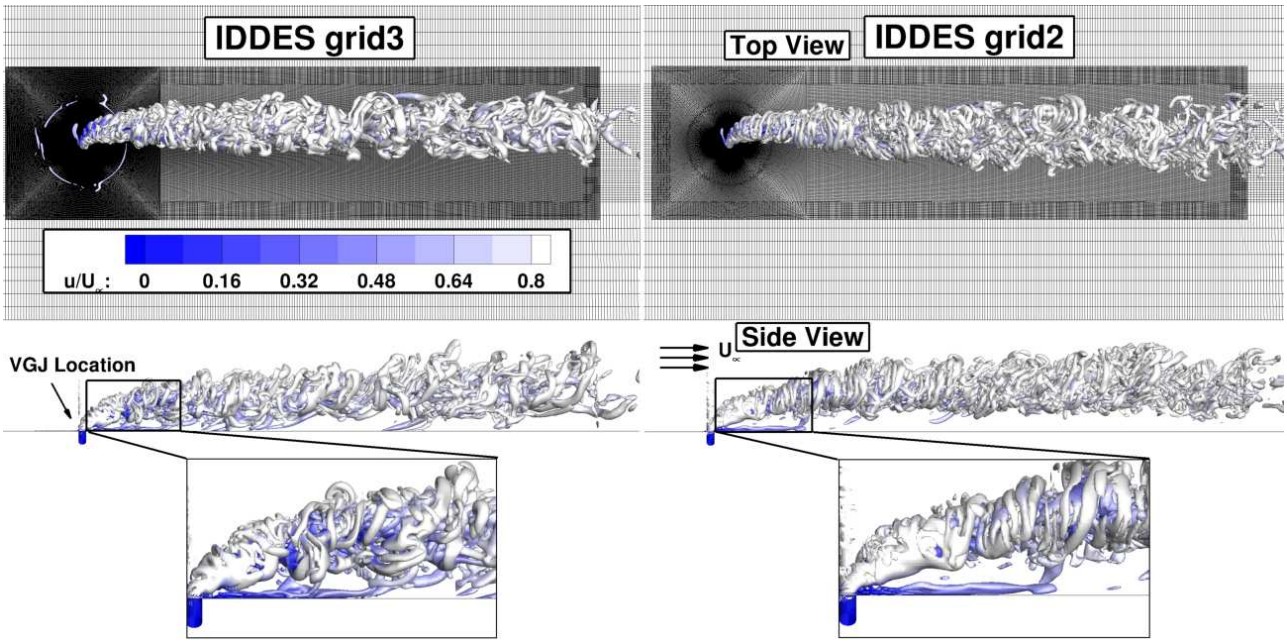

Fig. 9: Iso-Surface of the Q-criterion coloured by the normalized stream-wise velocity computed on grid2 and grid3.

IDDES grid2 predicted weaker span-wise velocities. Next the S-A RANS and IDDES grid2 results showed much higher wall-normal velocities in comparison with the MSST RANS and IDDES grid3. Again, the IDDES grid3 results are in good agreement with the experiments. Fig. 11 shows the effect of grid refinement by extracting the local velocity profiles at $x/\delta = 0.571$ in the wall-normal direction at $z/\delta = 0.058$, where y/δ, u/U_∞ and v/U_∞ represent the normalized span-wise direction, stream-wise and span-wise velocities respectively. The velocity profiles show that the vortex core in the decelerated region is well represented by the IDDES grid3 and also the bending characteristics of the stream-wise vortex is predicted accurately.

B. Unseady Vortex Motion and Figures of Merit

As mentioned earlier, an unsteady behavior of vortex centre was observed in the experiments downstream of the VGJ. This is a flow feature to be analyzed by the DES computation while the Unsteady RANS results show no signs of unsteady vortex motion. Therefore Fig. 12 shows that the IDDES model reproduces the unsteady motion of vortex centre similar as observed in the experiments at $x/\delta = 0.571$ downstream of the VGJ. It can be seen that the three grids used for the DES computations all predicted the unsteady vortex behavior. But the strongest vortex motion was obtained with grid3 and the range of vortex core positions matches well the experimental range. This suggests that satisfactory results are obtained through reasonable grid refinement in the LES region for such flow topologies. Table II shows the spatial postion of the vortex core predicted by the numerical results and compared with the experiments. Again, it can be stated that the IDDES grid3 results proved to be superior against the other RANS models and IDDES grid1 and grid2 results. Fig. 13 shows

TABLE II: Vortex core position at $x/\delta = 0.571$ downstream of VGJ

vortex core position	y/δ	z/δ
Experiment	0.10	0.174
S-A RANS	0.11	0.28
MSST RANS	0.107	0.20
IDDES grid1	0.125	0.30
IDDES grid2	0.119	0.28
IDDES grid3	0.104	0.173

the comparison of the numerically predicted dimensionless near-wall momentum coefficient ΔR_{Vx} at $x/\delta = 0.571$. The RANS predictions show a good overall agreement with the experiment among which MSST model predicts the vortex core region better than the S-A model. On the other hand, the MSST model over-predicts the ΔR_{Vx} value near to the wall compared to the experiments while S-A model shows better agreement. The DES predictions showed that successive grid refinement in the detached region gives accurate results as predicted by grid3. The DES results with grid3 showed promising results not only in the vortex core position but also the figure of merit for AFC, ΔR_{Vx}, agrees well in comparison to the experiment.

V. Conclusion

The numerical predictions showed that it is possible to simulate AFC devices using RANS and DES approaches in combination with Chimera grids. The Chimera grids proved useful in regions with local grid refinement independent of the global grid and it allowed to use very dense grids in the vicinity of VGJ to resolve small turbulent scales. RANS results predicted an overall good agreement with the experiments, where MSST

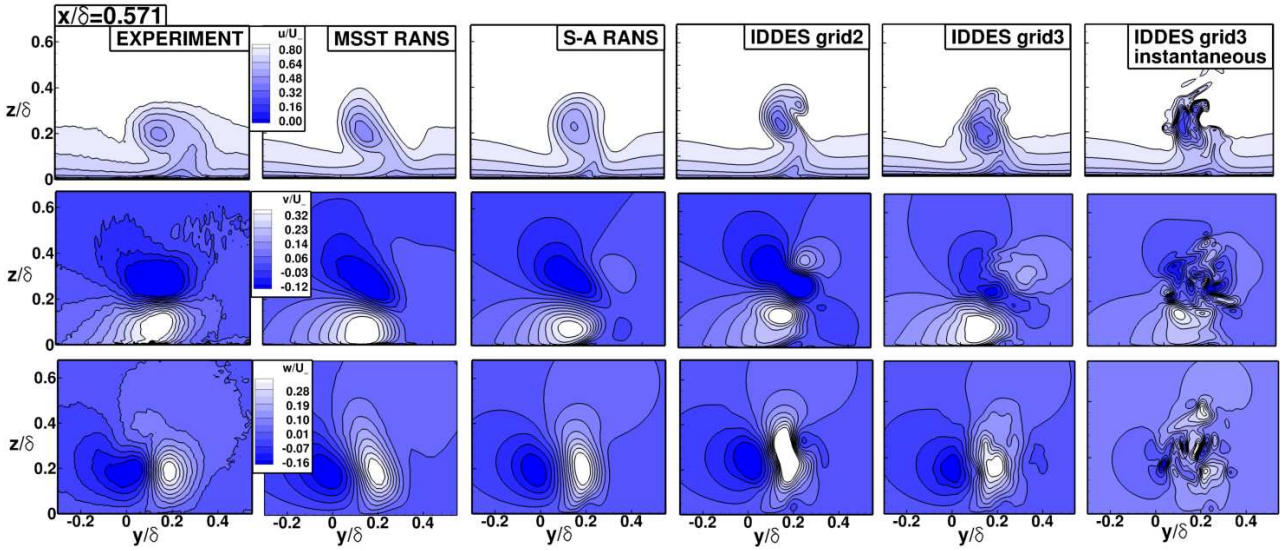

Fig. 10: Normalized velocity contours downstream of the VGJ.

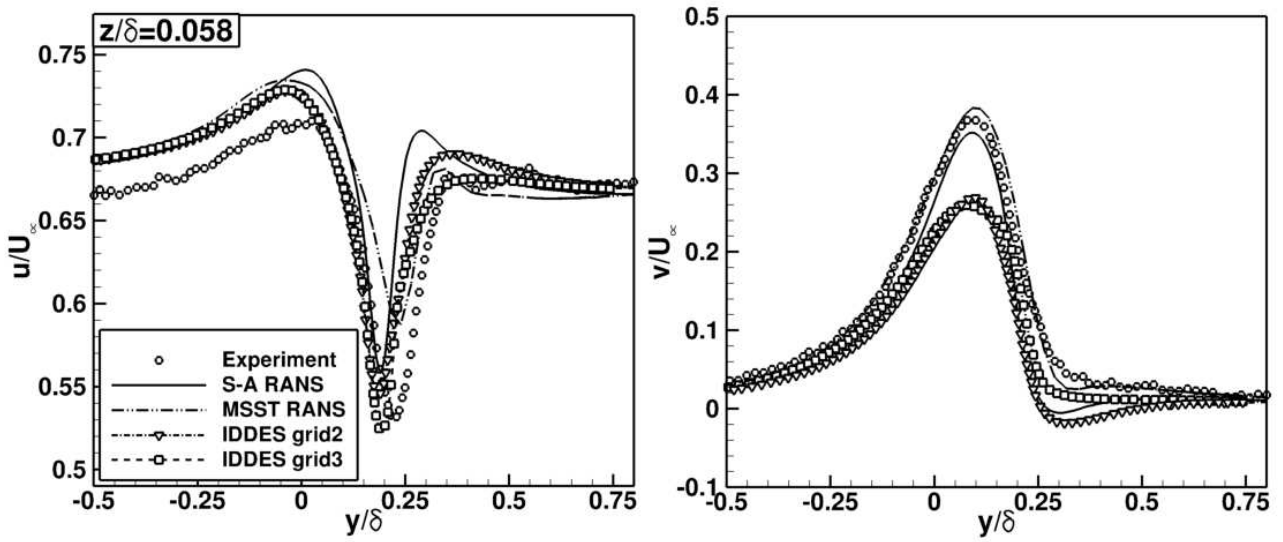

Fig. 11: Locally extracted details via velocity profiles at $x/\delta = 0.571$.

model showed better agreement with the measurment than the S-A model. The DES predictions on the other hand could represent the vortical motion of the VGJ and various turbulent length scales can be resolved by sufficient grid points in the LES region. The IDDES results show good agreement with the experiments in terms of the figure of merit, ΔR_{V_x}. The IDDES predictions reproduced the unsteady vortex motion observed in the experiments due to local grid refinement in the LES (detached) region. Therefore, it can be concluded that the IDDES model predicts the vortex-core position acccurately in comparison with the experiments and better than RANS. Note that the coarser IDDES grid1 and grid2 results showed disagreement due to less resolved turbulence. The improved numerical simulation of flow physics comes with a much higher computational effort, however. One IDDES simulation for 10 CR's requires an effective computing time of about 960 hours whereas a converged computation with the MSST RANS model can be performed with 10 hours.

Acknowledgment

The authors thank Dr. T. Schwarz, DLR, and A. Raichle, DLR, for his support in operating the TAU code with Chimera grids. Extensive discussions with A. Probst (TU Braunschweig) and Dr. K. Weinmann, DLR, related to the IDDES scheme used in the present work are gratefully acknowledged. Furthermore, the authors would like to thank Heribert Bieler and Burkhard Gölling (both Airbus Operations GmbH) for their ongoing interest and support. The research work was performed within the framework of 4th German Aeronautics Research Program (LuFo IV) in the project M-Fly AeroNext

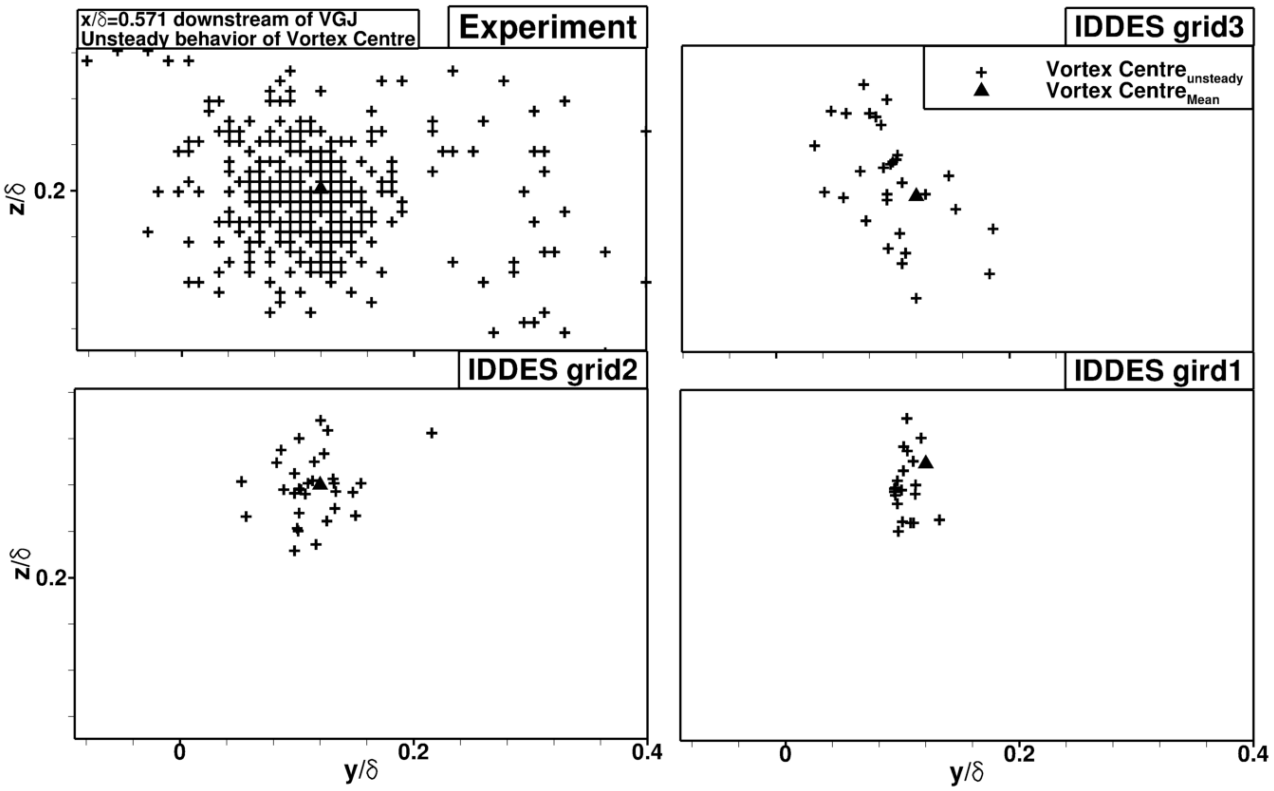

Fig. 12: Unsteady motion of vortex centre downstream of VGJ

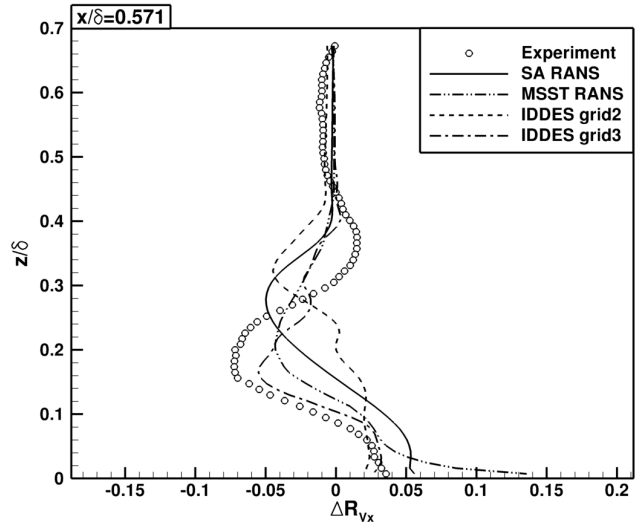

Fig. 13: Figures of merit ΔR_{V_x} at x/$\delta = 0.571$ downstream of VGJ

(coordinated and funded by Airbus Operations GmbH). High Performance Computing Resources were made available by HLRN.

REFERENCES

[1] X. Zhang, Co and Contrarotaing Streamwise Vortices in a Turbulent Boundary Layer, Journal of Aircraft, September-October 1995, Vol. 32, No. 5, pp. 1095-1101.
[2] J. Ortmanns, C.J. Kähler, A Single Round Vortex Generator Jet at High Reynolds Number, FLUCOME 2007, Tallahassee, Florida, USA.
[3] J. Ortmanns, Aktive Grenzschichtbeeinflussung mittels pneumatischer Wirbelgeneratoren bei groen Reynoldszahlen, Institut für Strömungsmechanik, TU Braunschweig, Dissertation ZLR-Forchungsbericht 2009-03.
[4] S. Mahmood, R. Radespiel, RANS simulation of jet actuation in a boundary layer flow using Chimera grids, Deutscher Luft- und Raumfahrtkongress 2009, September 8-10, Aachen, 2009.
[5] P. R. Spalart, Young person's guide to detached-eddy simulation grids, NASA CR-2001-211032.
[6] P. R. Spalart, S. Deck, M. Shur, K.D. Squires, M. Strelets, A. Travin, A new version of detached-eddy simulation, resistant to ambiguous grid densities, Theoretical and Computational Fluid Dynamics, Vol. 20, No. 3, pp. 181-195, 2006.
[7] S. Deck, E. Garnier, Detached and large eddy simulation of unsteady side-loads over an axisymmetric afterbody. Proceedings of 5th European Symposium on aerothermodynamics for space vehicles. Cologne, Germany, November 8-11, 2004.
[8] C. P. Mellen, J. Fröhlich, W. Rodi, Lessons from the European LESFOIL project on LES of flow around an airfoil, AIAA Journal, Vol. 41, No. 4, pp. 573-581, 2003.
[9] A. Travin, M. Shur, P.R. Spalart, M. Strelets, Improvement of delayed detaced-eddy simulation for LES with wall modelling, ECCOMAS CFD 2006. In: Wesseling, P., Oñate,E., Périaux, J. (Eds.), Proceedings (CDROM) of the European Conference on Computational Fluid Dynamics ECCOMAS CFD 2006, Egmond aan Zee, The Netherlands.
[10] M. Shur, P. R. Spalart, M. Strelets, A. Travin, A hybrid RANS-LES approach with delayed-DES and wall-modelled LES capabilities, International Journal of Heat and Fluid Flow 29 $(2008)1638 - 1649$.
[11] P. R. Spalart, W.-H. Jou, M. Strelets, S.R. Allmaras, Comments on the feasibility of LES for wings, and on a hybrid RANS/LES approach,

First AFOSR International Conference on DNS/LES, August 4-8, 1997, Ruston, Louisiana.
[12] P. R., Spalart, Strategies for turbulence modelling and simulations, Int. J. Heat Fluid Flow, 21, 252−263 (2000).
[13] M. Strelets, Detached Eddy Simulation of massively separated flows, AIAA Paper, $AIAA-2001-879$ (2001).
[14] T. Gerhold, O. Friedrich, J. Evans, M. Galle, Calculation of Complex Three-Dimensional Configurations Employing the DLR TAU-Code, 1997, AIAA-paper 97-0167.
[15] D. Schwamborn, T. Gerhold, R. Heinrich, The DLR TAU-Code: Recent applications in research and industry, ECCOMAS CFD 2006 CONFERENCE, September 04-08, 2006, Netherlands.
[16] A. Madrane, A. Raichle, A. Stuermer, Parallel implementation of a dynamic overset unstructured grid approach, ECCOMAS 2004, Jyväskylä, July 24-28, 2004.
[17] T. Schwarz, An Interpolation Method Maintaining the Wall Distance for Structured and Unstructured Overset Grids. In: Proceedings of the CEAS 2009 conference. CEAS 2009 European Air and Space Conference, October 26-29, 2009, Manchester, UK.
[18] Commercial CFD software package by POINTWISE, Inc. http://www.pointwise.com/gridgen
[19] Norddeutscher Verbund für Hoch und Höchsleistungsrechnen, http://www.hlrn.de, 2011.
[20] P. Spalart, and S. Allmaras, A one-equation turbulence model for aerodynamic flows, La Recherche Aerospatiale, 1994, pp. 5-21.
[21] F. MENTER, Improved two-equation turbulence models for aerodynamic flows, 1992, Tech. Report TM 103975, NASA, NASA Langley Research Center, Hampton, VA 23681-2199.